HDL·CR· 77-025-1

Investigation of Pressure Oscillations

in Axi-Symmetric Cavity Flows

September 1977

Final Report - Phase I

Prepared by

Jet Propulsion Laboratory
California Institute of Technology
Pasadena, California

Under Contract

MIPR No. R-77-25

**U.S. Army Materiel Development
and Readiness Command**
HARRY DIAMOND LABORATORIES
Adelphi, Maryland 20783

SECURITY CLASSIFICATION OF THIS PAGE *(When Data Entered)*

REPORT DOCUMENTATION PAGE	READ INSTRUCTIONS BEFORE COMPLETING FORM

1. REPORT NUMBER HDL-CR-77-025-1	2. GOVT ACCESSION NO.	3. RECIPIENT'S CATALOG NUMBER

4. TITLE *(and Subtitle)* Investigation of Pressure Oscillations in Axi-Symmetric Cavity Flows	5. TYPE OF REPORT & PERIOD COVERED Feb 16, 1976 thru Sep 30, 1976
	6. PERFORMING ORG. REPORT NUMBER JPL Publication 77-68

7. AUTHOR(s) V. Sarohia P. F. Massier	8. CONTRACT OR GRANT NUMBER(s) MIPR R-77-25 NAS 7-100

9. PERFORMING ORGANIZATION NAME AND ADDRESS Jet Propulsion Laboratory California Institute of Technology Pasadena, California	10. PROGRAM ELEMENT, PROJECT, TASK AREA & WORK UNIT NUMBERS Program Element 62703A Project No. 1W162114AH73 Task DO, Work Unit 007A9

11. CONTROLLING OFFICE NAME AND ADDRESS Harry Diamond Laboratories 2800 Powder Mill Road Adelphi, MD 20783	12. REPORT DATE September 1977
	13. NUMBER OF PAGES 40

14. MONITORING AGENCY NAME & ADDRESS(if different from Controlling Office) NASA Resident Procurement Office - JPL 4800 Oak Grove Dr. Pasadena, CA 91103	15. SECURITY CLASS. (of this report) Unclassified
	15a. DECLASSIFICATION/DOWNGRADING SCHEDULE

16. DISTRIBUTION STATEMENT *(of this Report)*

Approved for public release; distribution unlimited.

17. DISTRIBUTION STATEMENT *(of the abstract entered in Block 20, if different from Report)*

18. SUPPLEMENTARY NOTES

DRCMS Code 62703A
HDL Project No. 304734

19. KEY WORDS *(Continue on reverse side if necessary and identify by block number)*

Cavity Flows
Pressure Oscillations in Cavities

20. ABSTRACT *(Continue on reverse side if necessary and identify by block number)*

An experimental investigation was conducted of subsonic turbulent flows over shallow, axi-symmetric cavities located downstream of the leading edge of a flat-nosed fuse contour and on an ellipsoidal nose contour. The objective was to evaluate cavity performance in terms of pressure oscillations inside the cavity for various cavity configurations and other pertinent parameters for various modes of cavity operation. Free-stream velocities over the contours ranged up to 650 ft/sec, and Reynolds numbers based on maximum

DD FORM 1473 EDITION OF 1 NOV 65 IS OBSOLETE

diameter of the contour ranged between 10^4 and about 10^6.

It was found that pressure signals at the base of the cavity for an oscillating cavity flow as high as 150 dB, referred to 20 $\mu N/m^2$, could be obtained and that a total acoustic power as high as 20 W was estimated. Furthermore, pressure oscillations existed for cavity depths as small as 0.050 in. It may be that this is not the minimum depth for which oscillations are generated, since the next smaller depth tested was 0.020 in. For the smallest depth, of 0.020 in., pressure oscillations in the cavity did not occur.

Cavity oscillations were more pronounced when the cavity was located in the favorable (negative) pressure gradient region of the axi-symmetric body. Instant spark shadowgraphs taken for both laminar and for turbulent boundary layer flow separation at the upstream cavity corner showed the presence of large, organized vortex structure. in the oscillating shear layer. Mean velocity measurements of an oscillating cavity shear layer indicated an entrainment rate, $\frac{d\Theta}{dX}$, as large as 0.046 as compared to a non-oscillating cavity shear layer entrainment $\frac{d\Theta}{dX} \simeq 0.021$, where Θ is the momentum thickness and X is the streamwise coordinate. The above large entrainment rates for a turbulent separated cavity flow appeared to have been caused by the presence of these organized large-scale vortex structures imposed on the flow by the oscillating cavity flow system.

1. INTRODUCTION

The phenomena associated with oscillations in flows over cavities have been observed over a range of shear flows and cavity configurations. The role of the shear layer in these sustained oscillations (Refs 1 to 8) is more complex in flows over shallow cavities which have a depth d $\sim$ length b of the cavity (Refs 1 and 6) than in deep cavities for which d >> b. In deep cavities, the shear layer has been observed to act as a forcing mechanism and the oscillation phenomenon in them is caused by an acoustic resonance in the depth mode (Ref 9). Previous experiments performed by the authors (Refs 5 and 6) showed that the oscillations in shallow cavities are not caused by acoustic resonance phenomena in the longitudinal direction. Instead, these oscillations result from propagating disturbances which are amplified along the cavity shear layer.

The flows over shallow cavities are of interest because, under certain flow and geometrical configurations, they result in strong periodic oscillations which modify the drag (Ref 10), and modify the heat transfer (Refs 11 and 12), and result in strong pressure oscillations inside the cavity (Refs 10, and 12 to 14), as well as in the production of sound (Refs 4 and 6).

Karamcheti (Ref 4) studied the acoustic field from two-dimensional cavities in the Mach number range between 0.25 and 1.5. It was observed that for a fixed Mach number and depth, the minimum width for producing oscillations with laminar flow separation at the upstream corner of the cavity was smaller than with turbulent flow separation. No detailed measurements were made of the manner in which the aerodynamic and geometric conditions influence the onset of the cavity flow oscillations. Experiments performed at low subsonic speed with laminar boundary-layer separation at the upstream cavity corner (Ref 5) showed that the onset of cavity flow oscillations was critically dependent on the boundary-layer flow conditions at the upstream cavity corner.
However, no such measurements were made for turbulent, separated cavity shear flows.

Although there have been many investigations of cavity flows, very little is known about the details of the cavity flow field for a turbulent, separated shear layer. A careful and systematic investigation of the onset of cavity oscillations would lead to significant information that would be important in designing cavities for a desired application. The information needed is the manner in which the organized velocity fluctuations in the cavity shear layer modify the entrainment of a turbulent separated shear layer at the upstream cavity corner. Such an investigation was undertaken, in which pressure measurements and hot-wire measurements were made; also, photographs were taken of the flow field in the vicinity of the cavity.

2. EXPERIMENTAL ARRANGEMENTS AND MEASUREMENTS

2.1 Model and Free-Jet Facility

Experiments have been performed on two axi-symmetric cavity flow models which had outside diameters, D, of approximately 2 and 2.2 in. The

2.0-in.-diam model with an ellipsoidal nose had provision for variation of depth, d, in steps together with a continuously adjustable width, b. This model was primarily used for flow visualization. Either laminar or turbulent boundary layers could be obtained at the upstream edge of the cavity.

The second model had a fuse nose shape as indicated in Figure 1. The cavity width, b, of this model could be changed in steps having values of 0.225, 0.3, 0.4, 0.45, and 0.5 in. For each width, four cavity depths, d, of 0.2, 0.1, 0.055, and 0.02 in. could be obtained. This model was tested in the potential core of a 7-in.-diam free-jet flow. Studies were conducted using free-jet velocities as high as 650 ft/sec. Throughout the present experiments of the fuse nose model, the leading edge of the cavity was fixed at $X_o = 2.5$ in. from the leading edge of the fuse nose. This model had provision for inserting a pressure transducer at the base of the cavity. To analyze cavity oscillations, a hot-wire probe could be inserted in the shear layer without disturbing the flow around the cavity. The probe was moved across as well as along the shear layer. Its location could be determined within 0.001 in.

An identical fuse nose shape model without a cavity was used to measure the wall static pressure distribution. These measurements were carried out over a range of velocities up to 500 ft/sec to determine the influence of Reynolds number on the pressure distribution. A total of 19 static pressure taps were spaced along the surface.

2.2 Instrumentation and Measurements

Constant temperature, hot-wire anemometry was used extensively to determine the frequency of cavity oscillation. The linearized dc output of the hot-wire was recorded on an X-Y plotter to measure the mean velocity in the cavity shear layer. The ac output signals of the hot wire, which are proportional to the velocity fluctuations in the cavity shear layer, were passed through a filter and then analyzed on an all-digital, real-time spectrum analyzer to determine the frequency contents of the u' cavity flow velocity fluctuations. The hot-wire output was recorded on an X-Y plotter and simultaneously displayed on an oscilloscope and photographed.

The pressure fluctuations of the flow inside the cavity were measured with a 1/8-in. pressure transducer which was flush-mounted on the base of the cavity. The rise time of this transducer was 2 μsec. The frequency response of the pressure transducer was from 2 to 40,000 Hz. The output of the pressure transducer was amplified 100 times and then passed through a filter to remove the component of the signal caused by the vibration of the system. The rms value of the pressure signal was measured on a time-averaging rms voltmeter. The signal was also analyzed on a spectrum analyzer to determine frequency distribution. From the values of the mean square pressure fluctuations inside the cavity, the power of the acoustic waves was estimated as a function of cavity flow for each cavity configuration.

2.3 Flow Visualization

Flow near the cavity was visualized by injecting a small amount of CO_2 gas from the inside of the cavity. Instant spark shadowgraphs were

taken using an electronic stroboscope. The duration of the flash was less than 0.3 μsec during which time the cavity flow was photographed. This time was short enough to "freeze" the motion of the cavity flow field.

3. EXPERIMENTAL RESULTS

3.1 Minimum Width for Oscillations to Occur

The effect of free-stream velocity on different cavity configurations was determined. Figure 1 shows the nomenclature used to express the dimensions and flow quantities. For a given flow, a minimum cavity width existed for which no strong cavity oscillations were present. Results of the instant output of the cavity shear layer velocity fluctuations and of the cavity pressure oscillations for $b < b_{min}$ when $U_\infty = 183$ ft/sec are shown in Figure 2(a). The lower hot-wire trace does show weak periodic velocity fluctuations, but they do not contribute to strong pressure fluctuations inside the cavity. Figure 2(b) shows traces for $b > b_{min}$ for the same free-stream velocity $U_\infty = 183$ ft/sec when the cavity flow was oscillating. The value of b_{min} was 0.25 in. By comparing the traces in Figure 2(a) with those in Figure 2(b), it is evident that the oscillations were strong and almost, but not purely, sinusoidal in nature. It should be noted that both vertical and horizontal scales were identical. When the spectra of u' and of p' were taken, higher harmonics of the fundamental were observed because of some superimposed non-linear u' and p' fluctuations. These higher harmonics in the spectrum of u' and p' should not be confused with the higher modes of cavity flow oscillations.

In the present investigation, the conditions that caused the onset of the cavity flow to oscillate were studied for a turbulent separated shear layer and were compared with the laminar boundary layer results of Reference 5. As for the laminar separated-flow case, the present turbulent flow results also show that the experimental results seem to fall on a single curve when plotted

$$\frac{b_{min}}{\delta_0} \sqrt{\frac{U_\infty \ \delta_0}{\nu}}$$

as a function of the non-dimensional depth, $\frac{d}{\delta_0}$. This is shown in Figure 3. For a given depth, $\frac{d}{\delta_0}$, and cavity flow conditions, U_∞ and δ_0, it was found that $b_{min_{turb}} > b_{min_{lam}}$. The value δ_0 is the shear layer thickness at the upstream corner of the cavity.

3.2 Cavity Flow Oscillation Frequency

Figure 4 shows the influence of free-stream velocity on the frequency of cavity oscillations for a cavity width b = 0.25 in. and a depth d = 0.2 in. The cavity flow began to oscillate at $U_{\infty_{min}} \approx 470$ ft/sec, and no periodic

pressure fluctuations existed for U_∞ < 470 ft/sec. As the free-stream velocity was increased, the cavity flow oscillation frequency increased almost linearly. Within the range of free-stream velocity, the cavity-flow oscillations remained <u>primarily</u> in the first mode, which corresponds to a non-dimensional frequency $\frac{fb}{U_\infty}$ of 0.4 to 0.6. Because of some non-linearity superimposed on the pressure signal, however, the Fourier transform of this signal indicates a comparatively small amount of energy in the second mode of cavity flow oscillation as shown in Figure 4. The second mode shown in Figure 4 (as well as in Figure 5, discussed below) had less than 10% of the total periodic energy and thus should not be confused with the cavity oscillation phenomenon in the second mode of operation. For the same depth, d = 0.2 in., when the cavity width was b = 0.3 in., as indicated in Figure 5, the cavity began to oscillate at a lower free-stream velocity of 414 ft/sec. At free-stream velocities up to 600 ft/sec, the cavity flow remained primarily in the first mode of operation. The frequency data for other cavity flow and geometrical configurations are given in Tables 1 to 10.

Figure 6 shows the result of the effect of free-stream velocity on non-dimensional frequency $\frac{fb}{U_\infty}$ for various depths of the cavities. The non-dimensional frequency decreases slowly with an increase in free-stream velocity but is independent of the depth of the cavity. The first mode occurs around a non-dimensional frequency of 0.4 to 0.5 and the second mode around $\frac{fb}{U_\infty}$ of 0.75 to 1.0.

3.3 Cavity Flow Induced Pressure Oscillations and Tone Energy

Results in Figure 7, for b = 0.3 in. and d = 0.1 in., are typical for the filtered rms pressure fluctuations normalized with the free-stream dynamic head $1/2\, \rho_\infty U_\infty^2$, which is shown as a function of free-stream velocity. It is apparent in Figure 7 that very little energy exists for low free-stream velocities, i.e., for velocities less than U_{min}.

Within the range of velocities tested, the cavity could convert as much as 1.5% of the free-stream dynamic head into tone energy. These pressure oscillations were due to the second mode of cavity flow oscillations.

Results for this configuration, when plotted in terms of sound pressure level for the tone produced by the second mode of the filtered cavity pressure oscillations, are indicated in Figure 8. Sound pressure levels as high as 150 dB were observed. It should be noted that overall sound pressure levels were as much as 10 to 15 dB above the filtered sound pressure level indicated in Figure 8. A typical set of spectra of the cavity pressure oscillation signals at three free-stream velocities is shown in Figure 9. The tone of the second mode is clearly evident at the two higher velocities.

3.4 Acoustic Power Generated Inside Cavity

An estimate was made of the available acoustic power of the pressure oscillations inside the cavity by assuming that the pressure fluctuations as

sensed by the pressure transducer were caused primarily by the plane acoustic waves. The term $p'^2/\rho_0 c_0$ gives the acoustic power in the cavity pressure fluctuations. The reader is referred to Ref. 15 (pp. 249-253) for a detailed analysis on the energy of sound waves. Results of this computation are tabulated in Tables 1 - 10 for various cavity widths and depths as a function of free-stream velocity U_∞. Figure 10 shows the available acoustic power inside the cavity for a cavity width of b = 0.3 in. and a depth of d = 0.055 in. as a function of U_∞. For a non-oscillating cavity flow configuration, i.e., $U_\infty \sim U_{\infty_{min}}$, very little acoustic power is available. As the free-stream velocity was increased beyond $U_\infty \simeq 420$ ft/sec, the cavity flow began to oscillate violently, resulting in an increase in the available acoustic power. As the velocity was increased even farther, the available acoustic power increased very rapidly to approximately 4 W. The experimental results in Figure 11 for b = 0.4 in. and d = 0.1 in. further show that the available acoustic power of approximately 20 W was estimated.

3.5 Flow Visualization

The flow was made visible by injecting CO_2 gas at the base of the cavity. Spark shadowgraphs were taken for both laminar and turbulent boundary layer flows which separated at the upstream corner of the cavity.

The shadowgraphs in Figure 12 for laminar-separated cavity flow show an organized large vortex structure which is almost independent of small-scale turbulent structure. By contrast, small-scale turbulence, in addition to large-scale structures, can be seen in the shadowgraphs for a separated turbulent boundary-layer flow in Figure 13. The small-scale structure in the turbulent separated mixing layer produced the superimposed non-linearity in the u' cavity velocity fluctuation signal. These photographs clearly indicate the basic similarity of the cavity flow structure for both laminar and turbulent separated boundary layer shear flows as seen in the vicinity of the cavity. For the laminar boundary flow, the hot-wire signals indicated a near-sinusoidal velocity fluctuation in the cavity shear layer.

3.6 Growth of Cavity Shear Layer

Mean velocity in the cavity flow with turbulent boundary layer was measured for various cavity configurations to determine the growth rate of the cavity shear layer. Detailed measurements were made with a fixed upstream Reynold's number, $Re_{\theta_0} = 1.60 \times 10^3$, and fixed depth, $\dfrac{d}{\theta_0} = 37.5$. From these mean velocity profiles, the momentum thickness θ as defined below was determined:

$$\theta = \int_{-\infty}^{\infty} \frac{U}{U_\infty} \left(1 - \frac{U}{U_\infty}\right) dy \ .$$

In carrying out the integration inside the cavity, the integration was terminated where $U(y)$ was approximately 5 to 7 % of the mean edge velocity, U_∞. In this region, the hot-wire measurements are very doubtful. Measurements of the growth rate of the cavity shear layer for $\frac{b}{\Theta_0} = 34.7$, $\frac{b}{\Theta_0} = 55.2$, and $\frac{b}{\Theta_0} =$ 83.5, which correspond to non-oscillating and oscillating cavity flows, respectively, are indicated in Figure 14. Also shown is the growth rate $\frac{d\Theta}{dX}$, which indicates the entrainment rate of the shear layer. This entrainment rate was approximately 0.021 for the non-oscillating turbulent cavity shear layer and increased to a value as high as $\frac{d\Theta}{dX} = 0.046$. This high entrainment rate of the shear layer seems to result from the presence of organized large-scale structures in the cavity shear layer, as shown above in Section 3.5. Similar results have been obtained for laminar separated cavity shear flows (Ref 5).

3.7 Static Pressure Distribution Measurements

For the computation of the boundary-layer growth over the fuse nose, a prerequisite is the pressure distribution over the body. This information can be used to predict b_{min}. Figure 15 indicates the pressure coefficient C_p as a function of streamwise distance s/D for $U_\infty \simeq 480$ ft/sec and $Re_D \simeq 5.43 \times 10^5$. The static pressure was almost equal to the stagnation pressure on the flat portion of the nose but dropped suddenly as expected at the corner of the nose. One can infer the existance of a small separation bubble at the corner. The static pressure recovers suddenly around $s/D \simeq 0.17$ where the flow attaches. Downstream of this attachment point, i.e., $s/D > 0.2$, the flow accelerates and the static pressure drops slowly.

A comparison of static pressure distribution on the fuse nose shape for various Reynolds numbers is shown in Figure 16. Within the range of the free-stream velocity tested, the pressure coefficient was independent of the Reynolds number.

NOMENCLATURE

b	Cavity width (Figure 1)
c_0	Ambient acoustic speed
$C_p \equiv \dfrac{p - p_\infty}{\frac{1}{2}\rho_\infty U_\infty}$	Pressure coefficient
dB	Sound pressure level $\equiv 10 \log_{10} \dfrac{\overline{p'^2}}{\overline{p'^2}_{ref}}$ decibel
d	Cavity depth (Figure 1)
D	Outside diameter of axi-symmetric body (Figure 1)
f	Frequency in Hz
p	Local static pressure on the body
p'	Pressure variation associated with propagating acoustic wave
$\tilde{p} \equiv \sqrt{\overline{p'^2}}$	Root mean square pressure fluctuation
R	Outside radius of the axi-symmetric body
Re_D, Re_{Θ_0}, Re_{δ_0}	Reynolds number based on body diameter, momentum thickness, boundary layer thickness
s	Streamwise position along the model surface from leading stagnation point
u'	Velocity fluctuations in X direction
U(y)	Mean velocity in X direction
U_∞	Free-stream velocity
X	Streamwise coordinate from upstream cavity corner
X_0	Location of upstream cavity corner from X = 0
y	Transverse coordinate

λ	Wavelength of the propagating disturbance in the shear layer
ρ_0	Density of ambient air
δ_0	Shear layer thickness at $X = 0$
θ_0	Shear layer momentum thickness at separation where $X = 0$
$\dfrac{fb}{U_\infty}$	Non-dimensional frequency

Subscripts

$(\ )_{min}$	Corresponds to the conditions for onset of cavity oscillations
$(\ )_{lam}$	Laminar flow condition
$(\ )_{turb}$	Turbulent flow condition

LITERATURE CITED

1. Dougherty, N. S., Jr., and Anderson, C. F., "An Experimental Study on Suppression of Edgetones From Perforated Wind Tunnel Walls," AIAA Paper No. 76-50, AIAA 14th Aerospace Sciences Meeting, Washington, D. C., Jan. 26-28, 2976.

2. Franke, M. E., and Carr, D. L., "Effect of Geometry on Open Cavity Flow-Induced Pressure Fluctuations," AIAA Paper No. 75-492, AIAA 2nd Aero-Acoustics Conference, Hampton, Va., March 24-26, 1975.

3. Heller, H. H., and Bliss, D. B., "The Physical Mechanism of Flow-Induced Pressure Fluctuations in Cavities and Concepts for Their Suppression," AIAA Paper No. 75-491, AIAA 2nd Aero-Acoustics Conference, Hampton, Va., March 24-26, 1975.

4. Karamcheti, K., "Sound Radiated from Surface Cutouts in High-Speed Flows," Ph.D. Thesis, California Institute of Technology, June 1956.

5. Sarohia, V., "Experimental Investigation of Oscillations in Flows Over Shallow Cavities," AIAA Paper No. 76-1 2, AIAA 14th Aerospace Sciences Meeting, Washington, D. C., January 26-28, 1976.

6. Sarohia, V., and Massier, P. F., "Control of Cavity Noise," AIAA Paper No. 76-528, 3rd Aero-Acoustics Conference, Palo Alto, Calif., July 20-23, 1976.

7. Wooley, J. P., and K. Karamcheti, "The Two-Dimensional Development of Flow in the Presence of Periodic or Random Fluctuations with Application to the Calculations of Cavity Tones," AFOSR-TR-76-0336, February 1976.

8. Wooley, J. P., and Karamcheti, K., "The Role of Jet Stability in Edgetone Generation," AIAA Paper No. 73-628, AIAA 6th Fluid and Plasma Dynamics Conference, Palm Springs, Calif., July 16-18, 1973.

9. East, L. F., "Aerodynamic Induced Resonance in Rectangular Cavities," Journal of Sound and Vibration, Vol. 3, pp. 277-287, 1966.

10. McGregor, W., and White, R. A., "Drag of Rectangular Cavities in Super-sonic and Transonic Flows Including the Effects of Cavity Resonance," AIAA Journal, Vol. 8, No. 11, pp. 1959-1964, Nov. 1970.

11. Haugen, R. L., and Dhanak, A. M., "Heat Transfer in Turbulent Boundary-Layer Separation Over a Surface Cavity," ASME Journal of Heat Transfer, pp. 335-340, November 1967.

12. Charwat, A. F., "An Investigation of Separated Flows - Part II: Flow in the Cavity and Heat Transfer," _Journal of the Aerospace Sciences_," Vol. 28, pp. 513-527, 1961.

13. Dunham, W. H., "Flow-Induced Cavity Resonance in Viscous Compressible and Incompressible Fluids," _Fourth Symposium on Naval Hydrodynamics, Ship Propulsion and Hydrodynamics_, Rept. ARC-73, Vol. 3, Office of Naval Research, Washington, D. C., 1962.

14. Heller, H. H., Holmes, D. G., and Covert, E. E., "Flow Induced Pressure Oscillations in Shallow Cavities," _Journal of Sound and Vibration_, Vol. 18, No. 4, pp. 545-552, 1971.

15. Landau, L. D., and Lifshitz, E. M., _Fluid Mechanics_, Pergamon Press, 1959.

TABLE 1

THE EFFECTS OF U_∞ ON $\tilde{p}$, ON ACOUSTIC POWER, AND ON CAVITY FLOW
OSCILLATION FREQUENCY FOR FIXED VALUES OF b = 0.198 in. AND d = 0.055 in.

VELOCITY, U_∞, ft/sec	$\tilde{p}$ psi	FREQUENCY, kHz	TOTAL POWER Watts
176.8	0.00567	No Cavity Oscillations	2.74×10^{-3}
204.7	0.00695		4.12×10^{-3}
229.1	0.00855		6.23×10^{-3}
248.6	0.00963		7.90×10^{-3}
283.4	0.01342		1.53×10^{-2}
324.6	0.0182		2.82×10^{-2}
341.4	0.0208		3.68×10^{-2}
366.5	0.0257		5.62×10^{-2}
389.7	0.0299		7.62×10^{-2}
411.4	0.0353		0.106
429.2	0.0406		0.140
457.8	0.0465		0.184
475.6	0.0524		0.234
498.7	0.0588		0.294
551.7	0.0829		0.586
587.2	0.0989		0.834
639.8	0.133		1.50

TABLE 2

THE EFFECTS OF U_∞ ON $\tilde{p}$, ON ACOUSTIC POWER, AND ON CAVITY FLOW
OSCILLATION FREQUENCY FOR FIXED VALUES OF b = 0.3 in. AND d = 0.055 in.

VELOCITY, U_∞, ft/sec	$\tilde{p}$ psi	FREQUENCY, kHz			TOTAL POWER Watts
		1st Mode	2nd Mode	3rd Mode	
147.3	0.00465				2.82×10^{-3}
207.6	0.00695				6.31×10^{-3}
239.1	0.00600				4.50×10^{-3}
275.2	0.00829				8.97×10^{-3}
310.3	0.0109				0.016
354.2	0.0157				0.032
429.2	0.0717				0.670
464.5	0.0824		14.7		0.885
563.9	0.0882		17.2		1.02
590.4	0.120		17.7		1.89
619.6	0.149		18.2		2.89
650.9	0.179		18.9		4.19

TABLE 3

THE EFFECTS OF U_∞ ON $\tilde{p}$, ON ACOUSTIC POWER, AND ON CAVITY FLOW
OSCILLATION FREQUENCY FOR FIXED VALUES OF b = 0.35 in. AND d = 0.055 in.

VELOCITY, U_∞, ft/sec	$\tilde{p}$ psi	FREQUENCY, kHz			TOTAL POWER Watts
		1st Mode	2nd Mode	3rd Mode	
218.6	0.00615				5.79×10^{-3}
279.3	0.0100				0.015
328.0	0.0121				0.022
372.5	0.0214				0.070
419.1	0.0331				0.168
462.3	0.0481				0.354
490.5	0.0695		13.1		0.740
553.5	0.0941		14.4		1.36
585.5	0.111		15.0		1.89
624.0	0.148		15.7		3.34
659.1	0.187		16.3		5.37

TABLE 4

THE EFFECTS OF U_∞ ON $\tilde{p}$, ON ACOUSTIC POWER, AND ON CAVITY FLOW

OSCILLATION FREQUENCY FOR FIXED VALUES OF b = 0.45 in. AND d = 0.055 in.

VELOCITY, U_∞, ft/sec	$\tilde{p}$ psi	FREQUENCY, kHz			TOTAL POWER Watts
		1st Mode	2nd Mode	3rd Mode	
207.6	0.00652				0.008
295.3	0.0137				0.037
328.0	0.0185				0.068
360.4	0.0230		13.9		0.105
411.4	0.0326		14.4		0.211
443.8	0.0412		14.9		0.337
473.4	0.0508		15.5		0.513
518.5	0.0674		16.3		0.903
553.5	0.0872	10.6	17.1		1.51
587.2	0.120	10.9	17.9		2.88
624.0	0.155	11.4	18.7	22.6	4.78
676.1	0.214	11.5	19.8	23.8	9.13

TABLE 5

THE EFFECTS OF U_∞ ON $\tilde{p}$, ON ACOUSTIC POWER, AND ON CAVITY FLOW

OSCILLATION FREQUENCY FOR FIXED VALUES OF b = 0.4 in. AND d = 0.055 in.

VELOCITY, U_∞, ft/sec	$\tilde{p}$ psi	FREQUENCY, kHz			TOTAL POWER Watts
		1st Mode	2nd Mode	3rd Mode	
275.2	0.00925			13.1	0.015
310.3	0.0135			13.6	0.032
347.9	0.0193			13.9	0.065
386.9	0.0299			-	0.157
453.2	0.0513			17.6	0.463
484.2	0.0615			18.1	0.665
510.7	0.0716			18.7	0.901
542.8	0.0834		12.3	19.7	1.22
579.0	0.0973		12.9	20.8	1.66
619.6	0.174		13.5	22.0	5.33
678.7	0.198		14.5	23.0	6.89

TABLE 6

THE EFFECTS OF U_∞ ON $\tilde{p}$, ON ACOUSTIC POWER, AND ON CAVITY FLOW

OSCILLATION FREQUENCY FOR FIXED VALUES OF b = 0.5 in. AND d = 0.055 in.

VELOCITY, U_∞,	$\tilde{p}$	FREQUENCY, kHz			TOTAL POWER
ft/sec	psi	1st Mode	2nd Mode	3rd Mode	Watts
218.6	0.0096				0.020
266.6	0.0144				0.046
306.6	0.0187				0.078
363.5	0.0310			13.9	0.214
384.1	0.0369				0.303
434.1	0.0658		12.0		0.964
471.2	0.0872		12.8		1.69
533.7	0.128		14.1		3.67
551.7	0.144		14.5		4.62
593.5	0.191		14.9		8.16
621.1	0.226		15.5		11.4
650.9	0.259		15.8		15.0

TABLE 7

THE EFFECTS OF U_∞ ON $\tilde{p}$, ON ACOUSTIC POWER, AND ON CAVITY FLOW

OSCILLATION FREQUENCY FOR FIXED VALUES OF b = 0.225 in. AND d = 0.1 in.

VELOCITY, U_∞, ft/sec	$\tilde{p}$ psi	FREQUENCY, kHz			TOTAL POWER Watts
		1st Mode	2nd Mode	3rd Mode	
306.6	0.018				0.0294
366.5	0.032		18.0		0.0978
426.7	0.053		20.0		0.264
455.5	0.064		21.1		0.389
516.6	0.088		22.9		0.735
557.0	0.115		24.1		1.26
585.5	0.131	13.0	25.0		1.63
613.6	0.158	13.3	NOT MEASURED		2.37
619.3	0.240	14.2	NOT MEASURED		5.47

TABLE 8

THE EFFECTS OF U_∞ ON $\tilde{p}$, ON ACOUSTIC POWER, AND ON CAVITY FLOW OSCILLATION FREQUENCY FOR FIXED VALUES OF b = 0.3 in. AND d = 0.1 in.

VELOCITY, U_∞, ft/sec	$\tilde{p}$ psi	FREQUENCY, kHz			TOTAL POWER Watts
		1st Mode	2nd Mode	3rd Mode	
287.4	0.0107		-		0.0145
351.1	0.0208		13.8		0.0551
381.2	0.0262		14.3		0.0874
414.0	0.0342		15.0		0.149
457.8	0.0513		16.3		0.335
494.6	0.0695		17.3		0.615
524.3	0.0887		18.0		1.00
563.9	0.116		18.9		1.71
595.1	0.141		19.7		2.56
631.3	0.174		20.5		3.85
674.8	0.226		21.8		6.49

TABLE 9

THE EFFECTS OF U_∞ ON $\tilde{p}$, ON ACOUSTIC POWER, AND ON CAVITY FLOW
OSCILLATION FREQUENCY FOR FIXED VALUES OF b = 0.35 in. AND d = 0.1 in.

VELOCITY, U_∞, ft/sec	$\tilde{p}$ psi	FREQUENCY, kHz 1st Mode	2nd Mode	3rd Mode	TOTAL POWER Watts
253.3	0.00856		-		0.0110
310.3	0.0137		9.7		0.0282
378.4	0.0246		11.4		0.0904
421.7	0.0278		12.4		0.116
455.5	0.0385		13.4		0.221
494.6	0.0650		14.4		0.631
565.6	0.149		15.7		3.32
609.1	0.193		16.6		5.54
6550.0	0.254		17.4		9.64

TABLE 10

THE EFFECTS OF U_∞ ON $\tilde{p}$, ON ACOUSTIC POWER, AND ON CAVITY FLOW

OSCILLATION FREQUENCY FOR FIXED VALUES OF b = 0.4 in. AND d = 0.1 in.

VELOCITY, U_∞, ft/sec	$\tilde{p}$ psi	FREQUENCY, kHz			TOTAL POWER Watts
		1st Mode	2nd Mode	3rd Mode	
270.9	0.0122		2		0.0255
321.1	0.0193		8.9	13.4	0.0635
384.1	0.0348		10.2	15.4	0.207
406.1	0.0480		10.7	16.5	0.395
453.2	0.0856		11.7	17.8	1.26
479.9	0.120		12.2		2.48
546.4	0.177		13.4		5.34
574.0	0.201		13.8		6.93
606.0	0.249		14.3		10.6
645.4	0.280		14.9		13.4
683.8	0.337		15.5		19.5
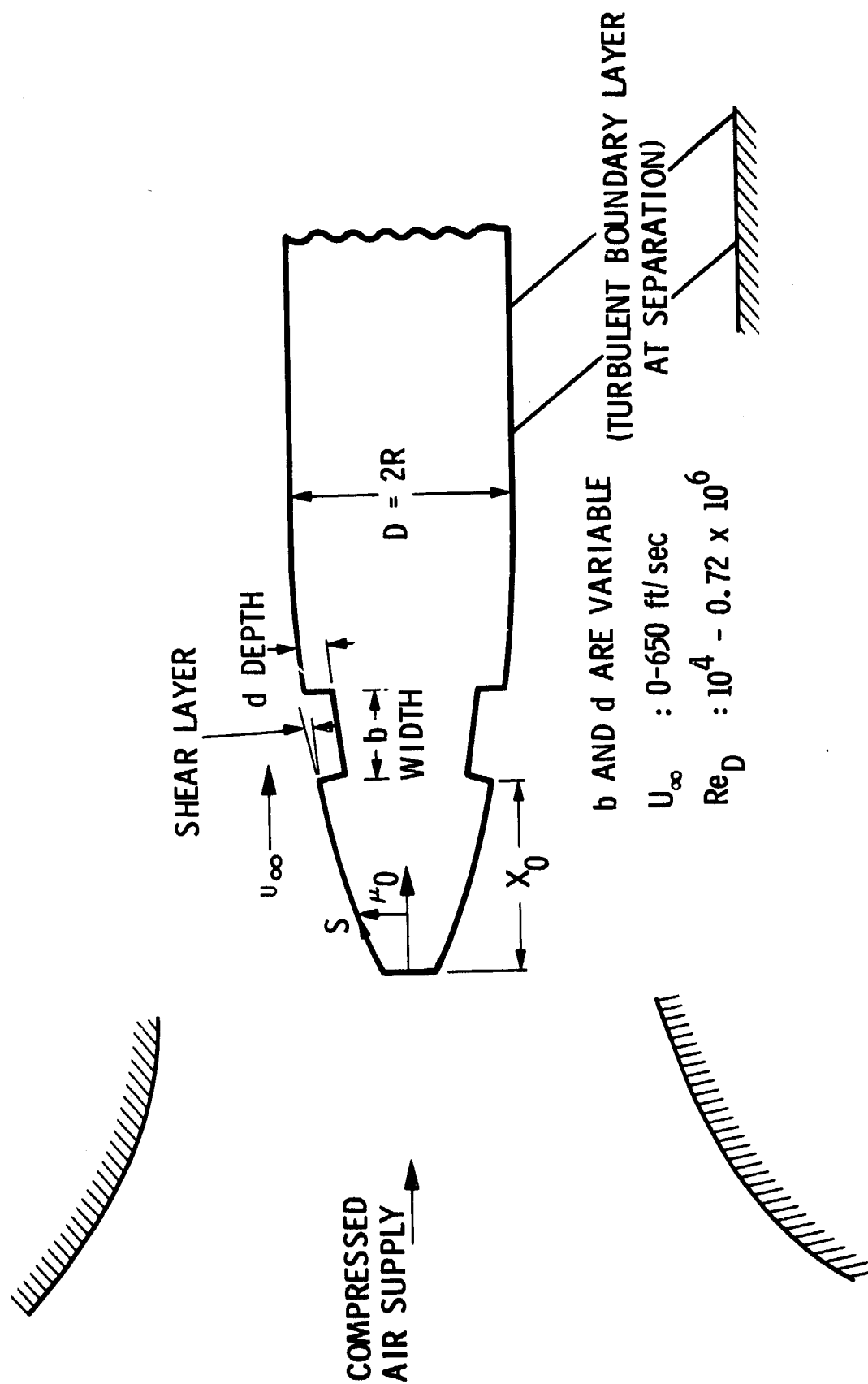
FIGURE 1. CAVITY OSCILLATION MODEL WITH PERTINENT NOMENCLATURE

U ≈ 183 ft/sec
DEPTH ≈ 0.25 in.
HORIZONTAL SCALE 50 μs/DIVISION

(a) $b < b_{min}$
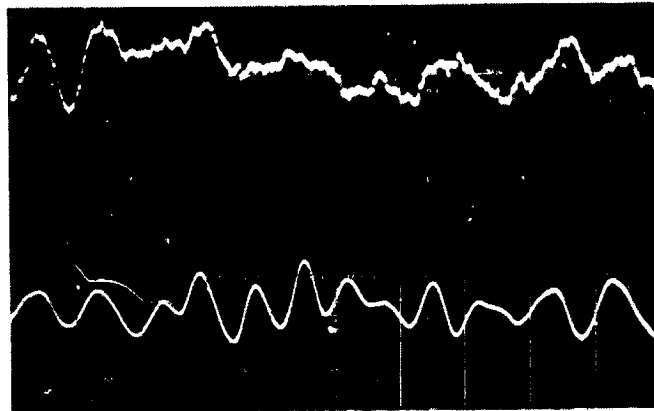
NON-OSCILLATING CAVITY CONFIGURATION
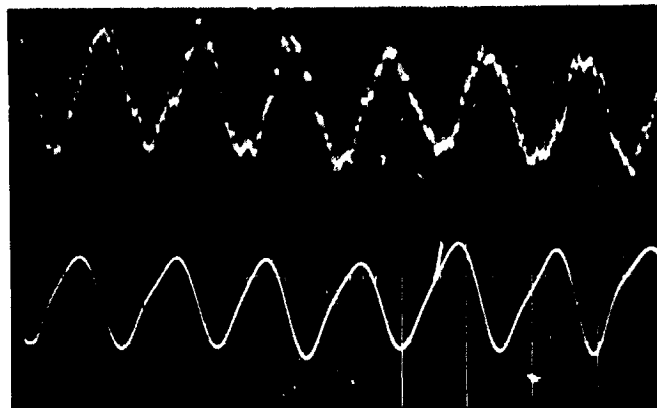
(b) $b > b_{min} = 0.25$ in.

OSCILLATING CAVITY CONFIGURATION

UPPER TRACE: PRESSURE TRANSDUCER SIGNAL INSIDE THE CAVITY

LOWER TRACE: HOT-WIRE SIGNAL IN CAVITY SHEAR LAYER

HORIZONTAL AND VERTICAL SCALES SAME IN ALL TRACES

FIGURE 2.   OSCILLOSCOPE TRACES OF CAVITY OSCILLATIONS
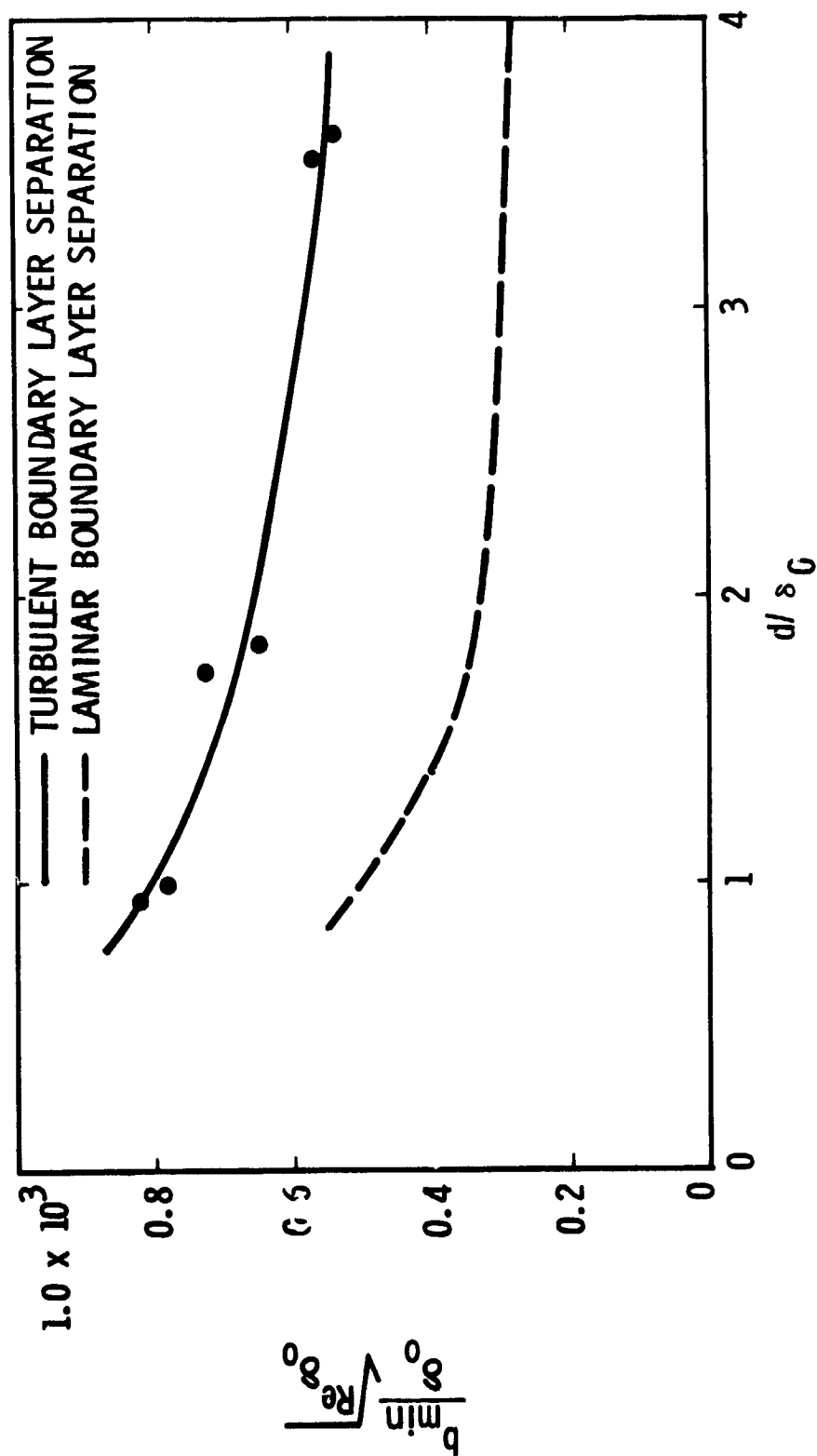
FIGURE 3. REGIONS OF CAVITY OSCILLATIONS
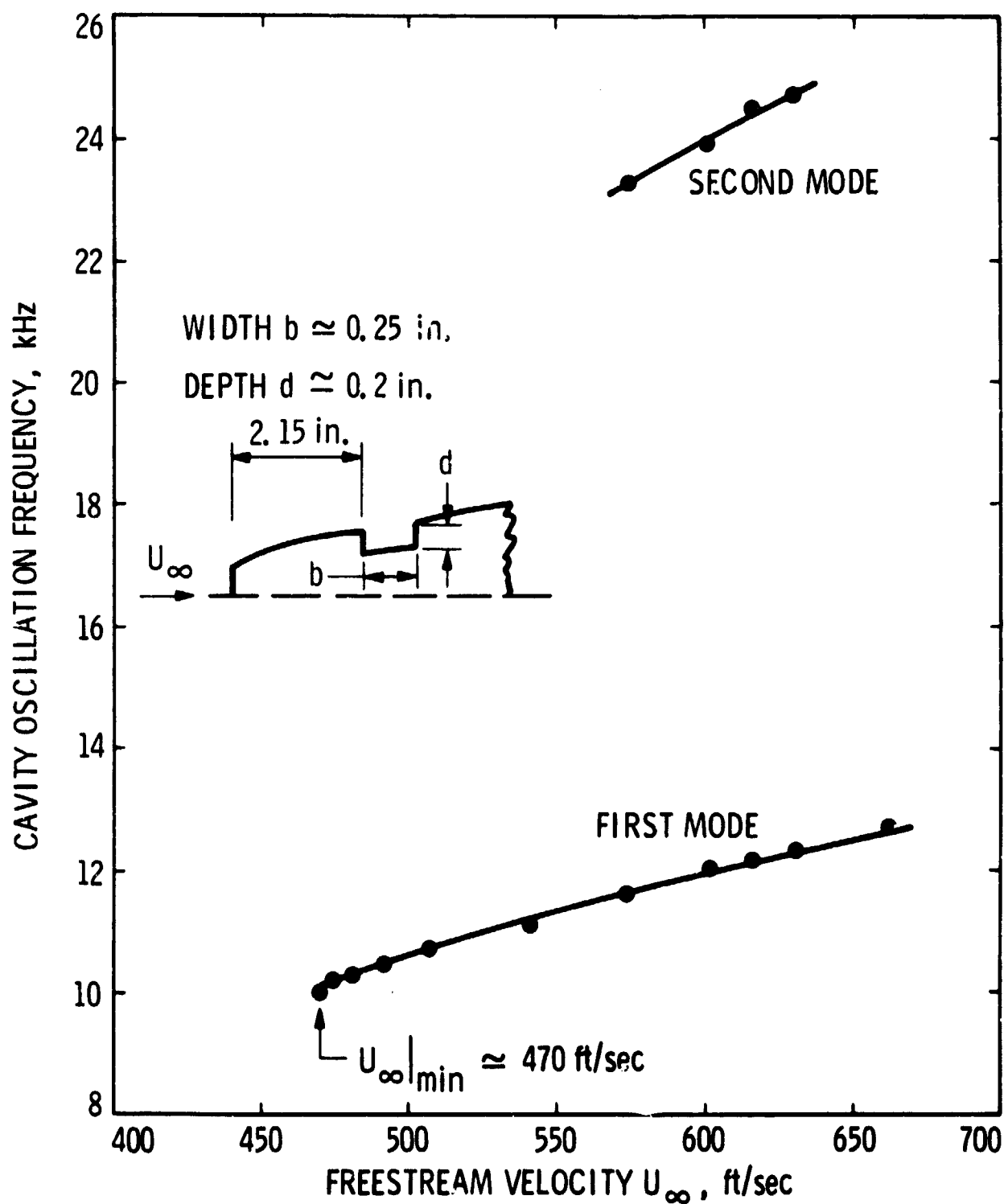
FIGURE 4. EFFECT OF FREESTREAM VELOCITY ON FREQUENCY OF CAVITY FLOW OSCILLATIONS FOR FIXED CAVITY WIDTH b = 0.25 IN. AND DEPTH d = 0.2 in.
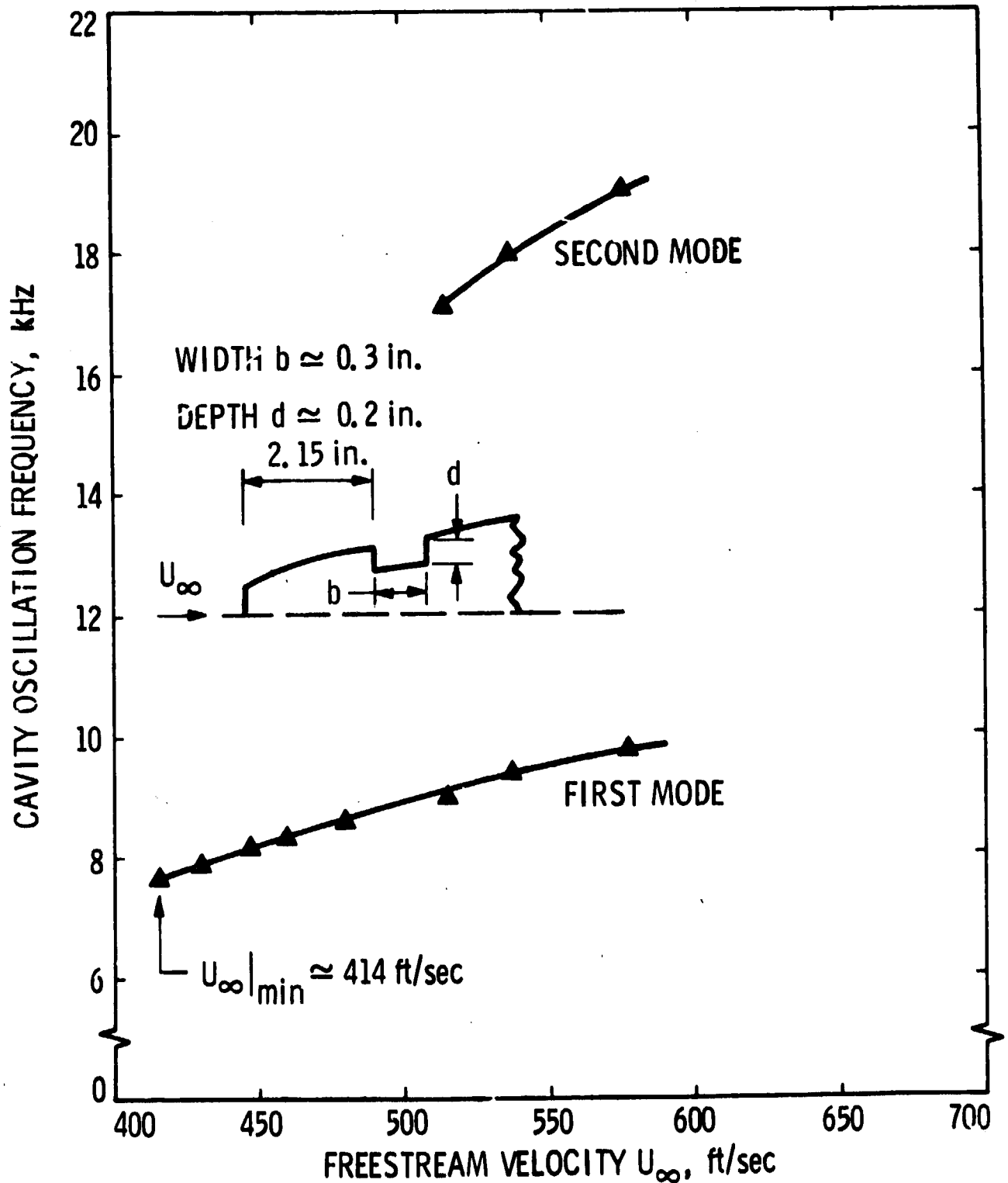
FIGURE 5. EFFECT OF FREESTREAM VELOCITY ON FREQUENCY OF CAVITY FLOW OSCILLATIONS FOR A FIXED CAVITY WIDTH b = 0.3 IN. AND DEPTH d = 0.2 IN.
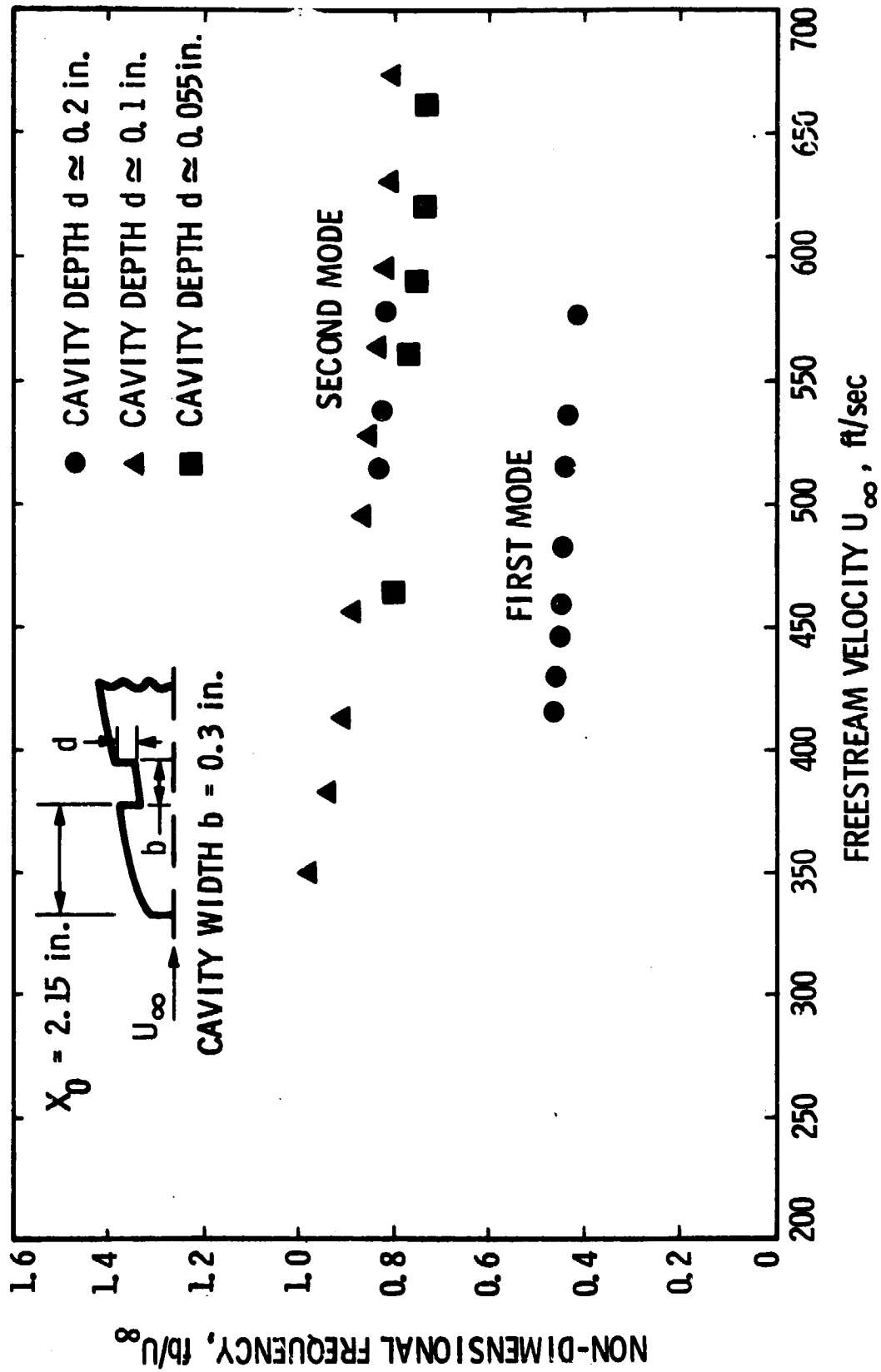
FIGURE 6. EFFECT OF FREESTREAM VELOCITY ON NON-DIMENSIONAL FREQUENCY
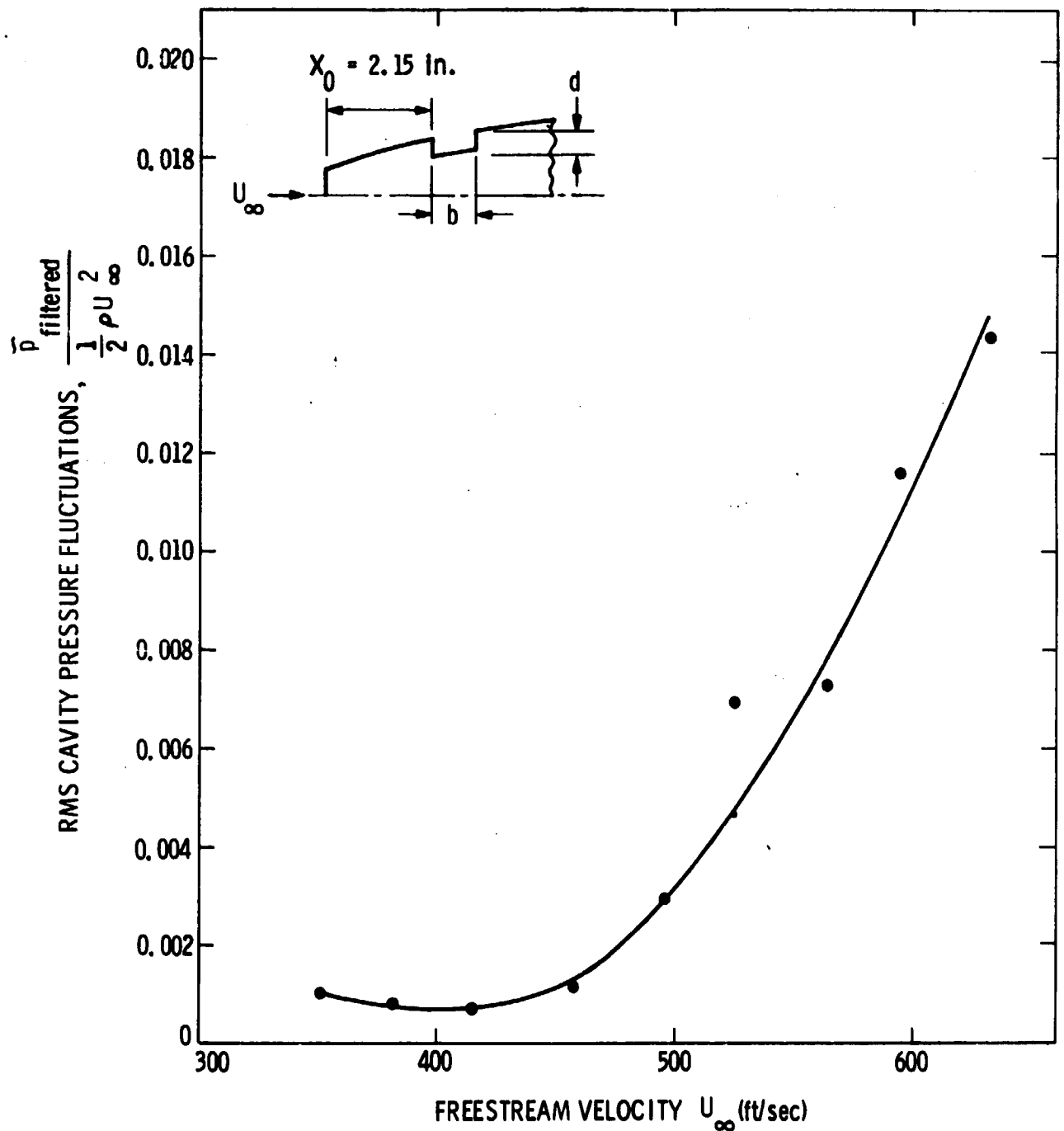
FIGURE 7.   INFLUENCE OF FREESTREAM VELOCITY ON CAVITY PRESSURE FLUCTUATIONS FOR CAVITY
WIDTH b = 0.3 IN. AND DEPTH d = 0.1 IN.
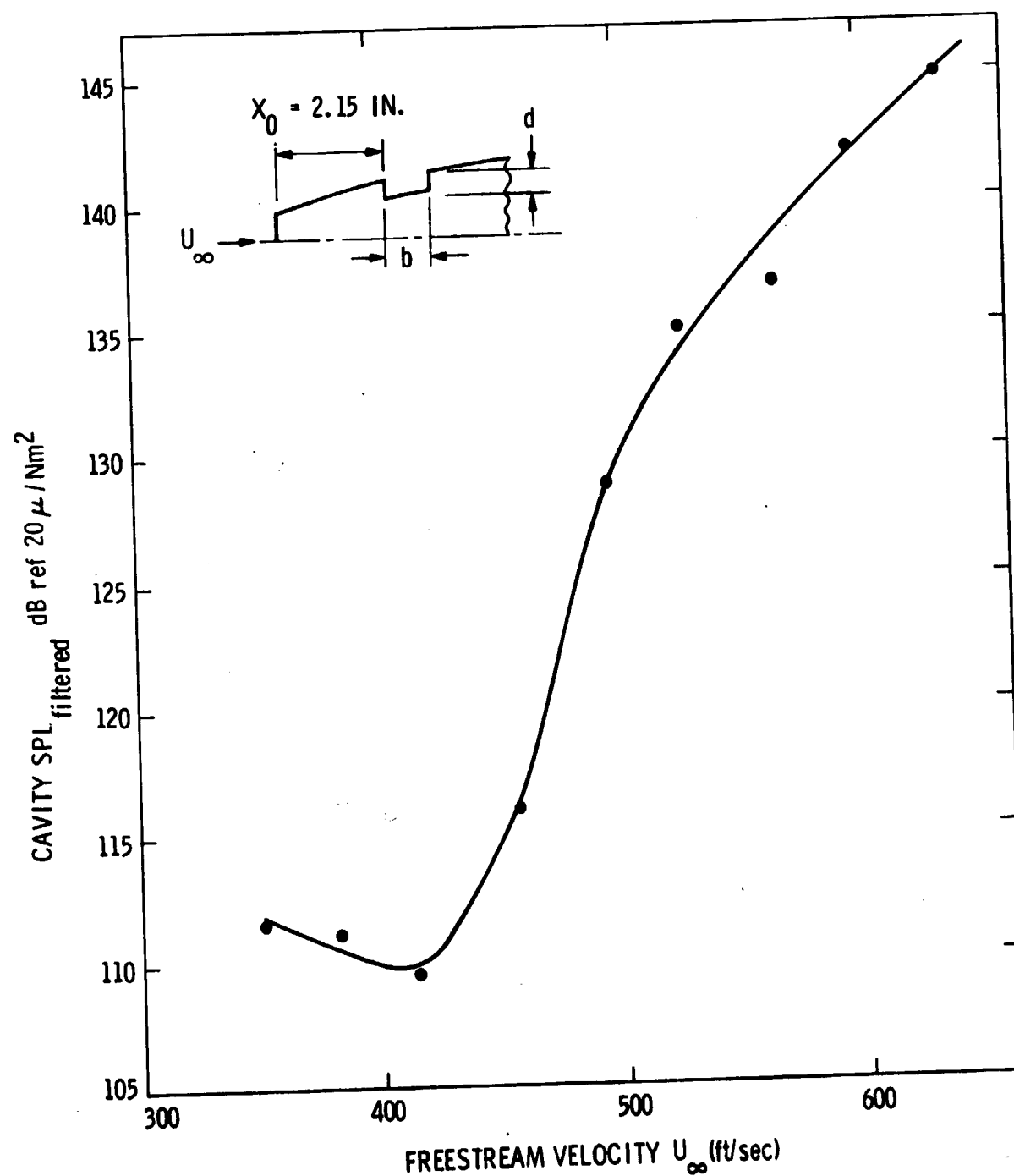
FIGURE 8. EFFECT OF FREESTREAM VELOCITY ON CAVITY SOUND PRESSURE LEVEL FOR
WIDTH b = 0.3 IN. AND DEPTH d = 0.1 IN.

FREESTREAM VELOCITY
U_∞ = 381 ft/sec
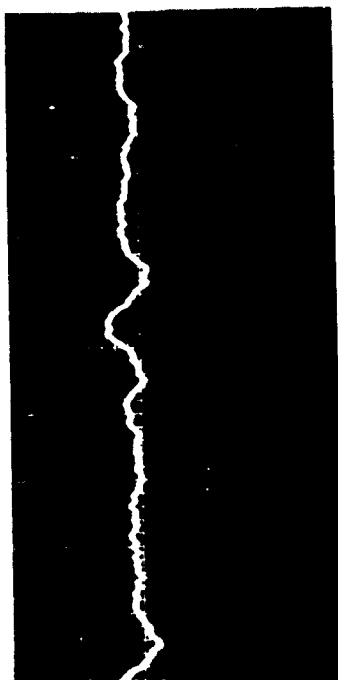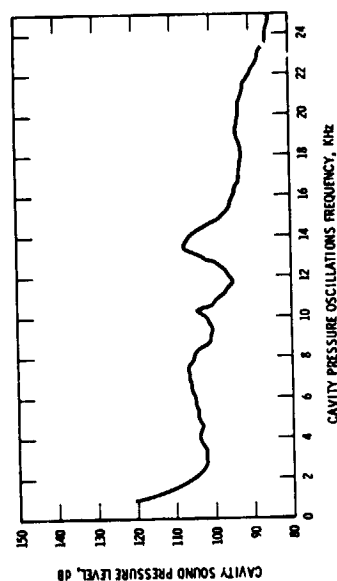
FREESTREAM VELOCITY
U_∞ = 458 ft/sec
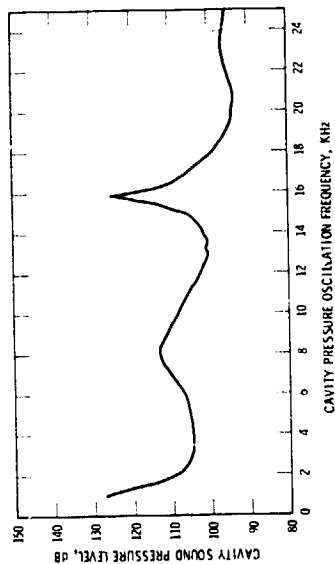
FREESTREAM VELOCITY
U_∞ = 595 ft/sec
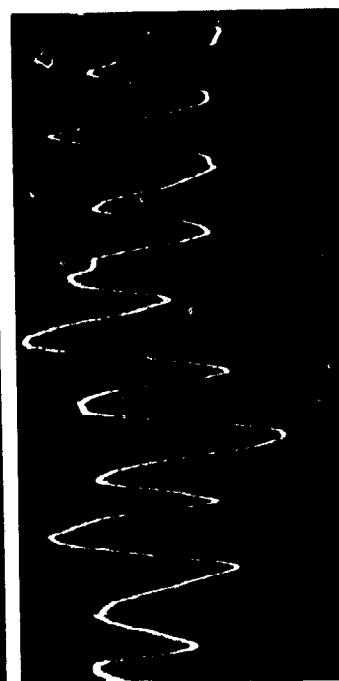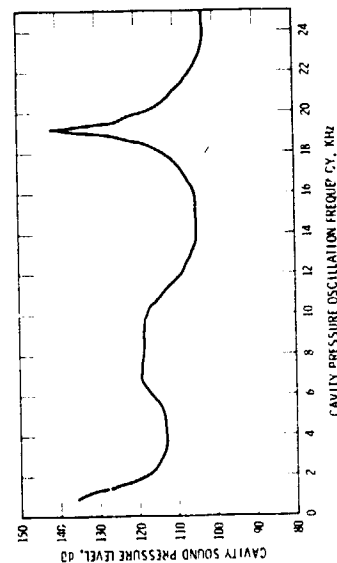
HORIZONTAL SCALE 50 μs/DIVISION
HORIZONTAL AND VERTICAL SCALES SAME ON ALL TRACES

FIGURE 9. SPECTRUM OF CAVITY PRESSURE OSCILLATIONS AT VARIOUS FREESTREAM VELOCITIES
FOR A FIXED WIDTH b = 0.3 IN. AND DEPTH d = 0.1 IN.
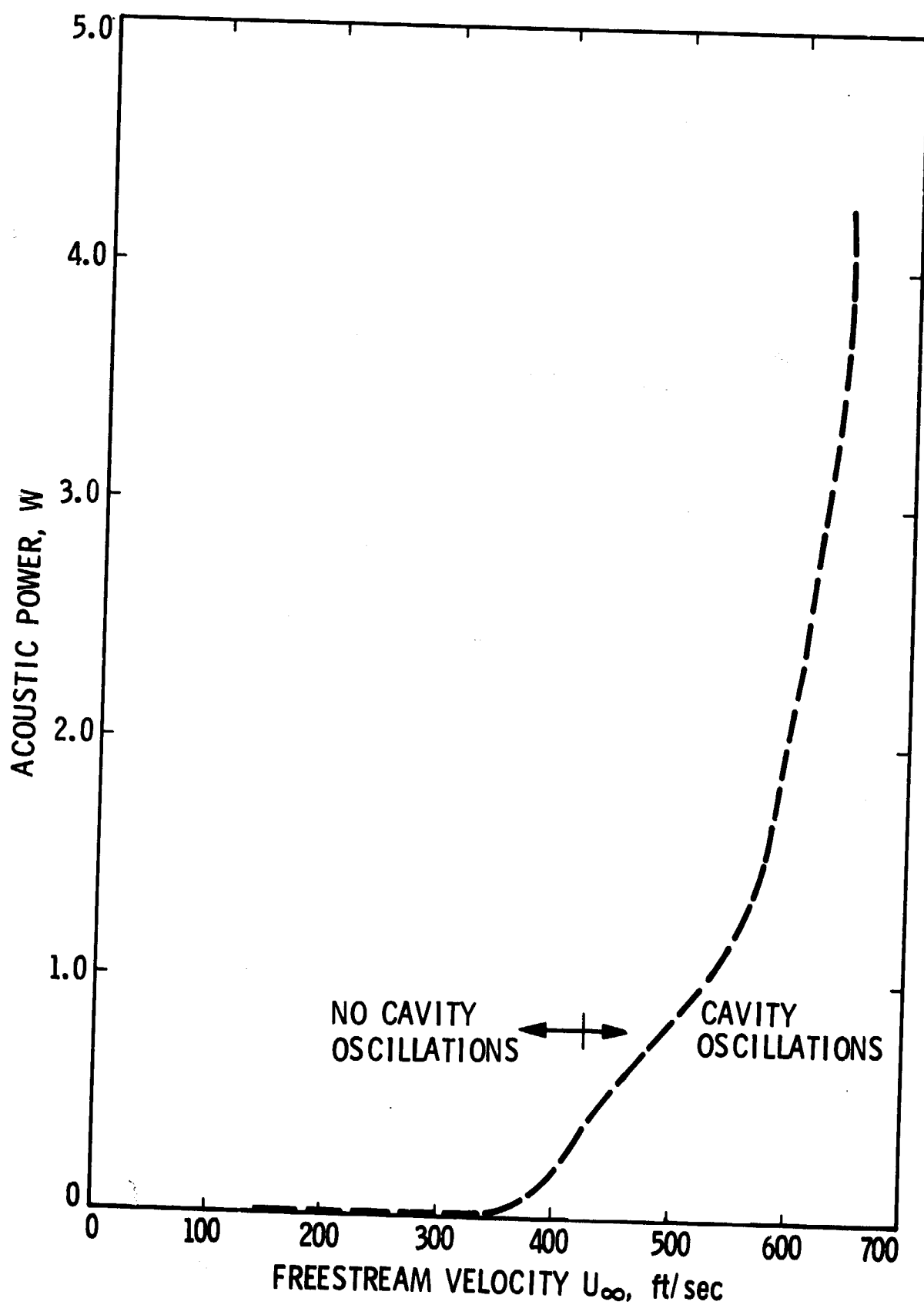
FIGURE 10.   INFLUENCE OF FREE-STREAM VELOCITY ON CAVITY ACOUSTIC POWER FOR A FIXED
CAVITY WIDTH b = 0.3 IN. AND DEPTH d = 0.055 IN.
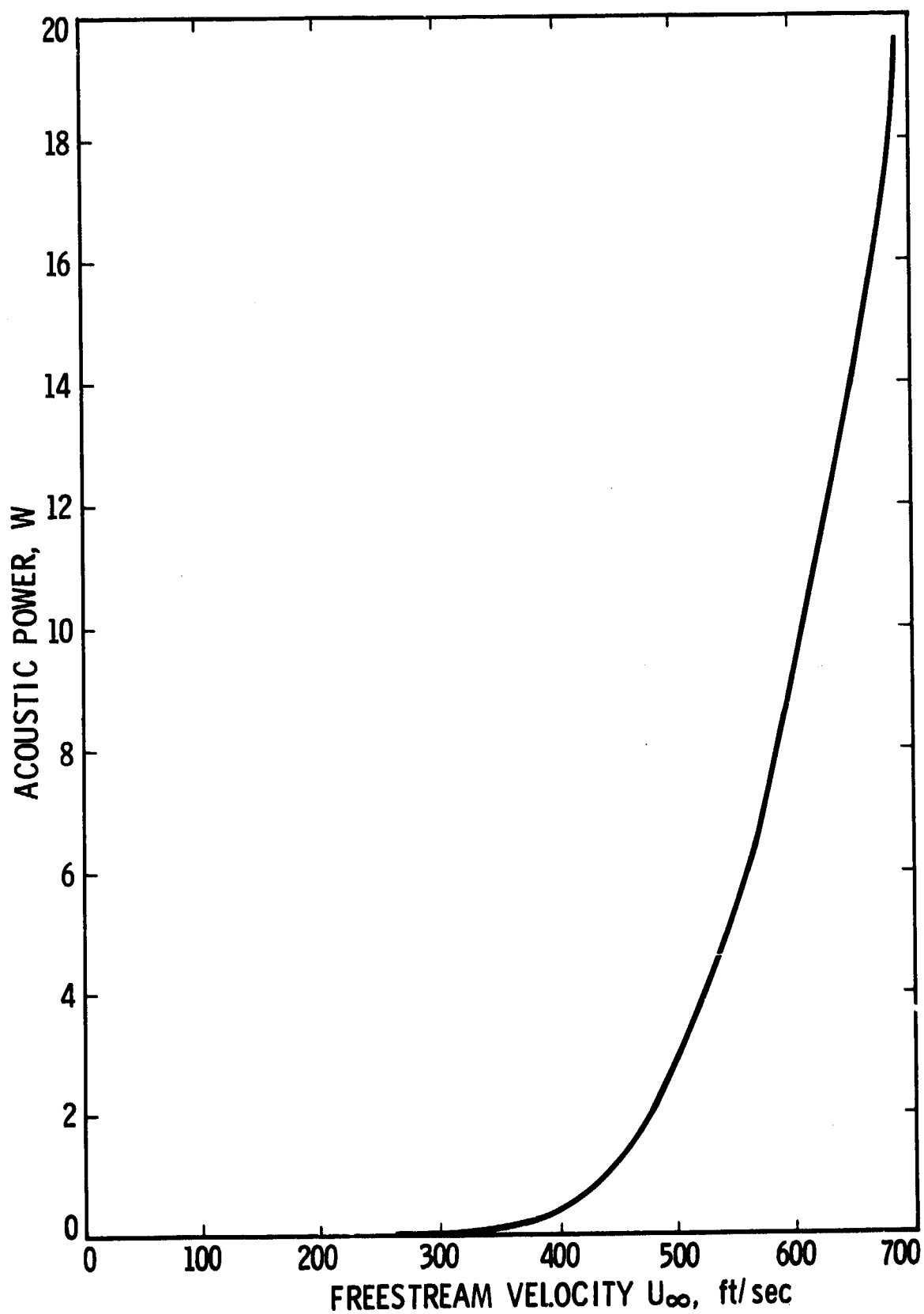
FIGURE 11.   INFLUENCE OF FREE-STREAM VELOCITY ON CAVITY ACOUSTIC POWER FOR A FIXED
WIDTH b = 0.4 IN. AND DEPTH d = 0.1 IN.
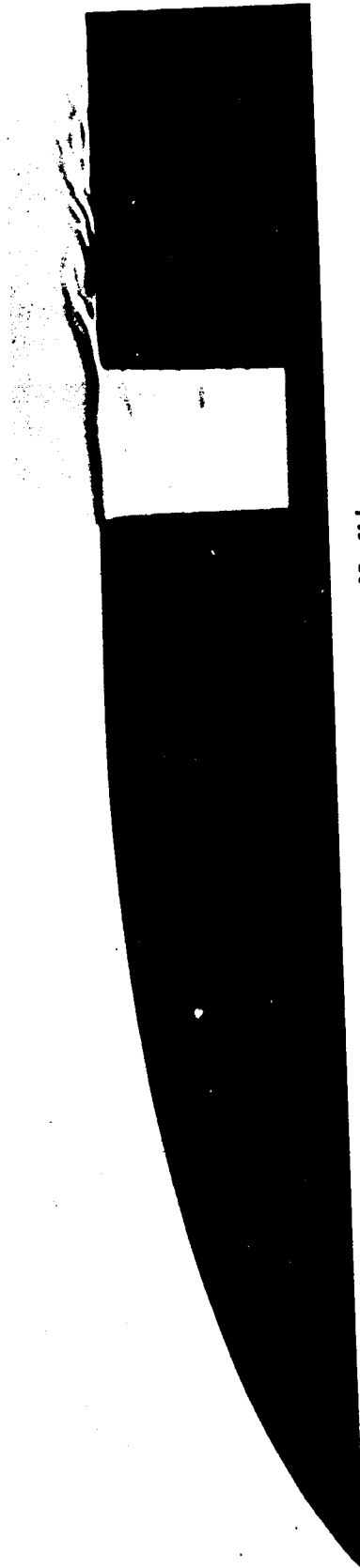
(a) FREESTREAM VELOCITY U_∞ = 41 ft/sec
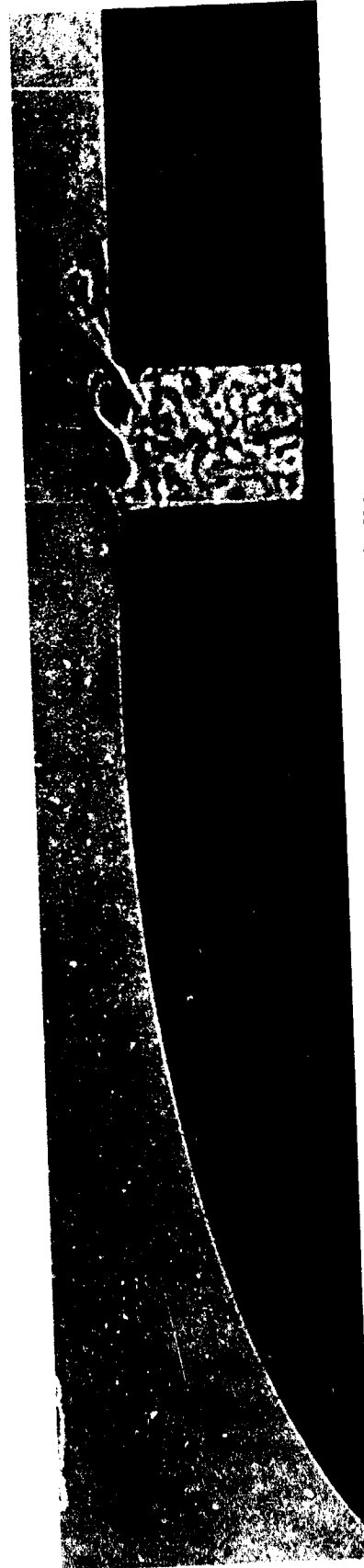
(b) FREESTREAM VELOCITY U_∞ = 96 ft/sec

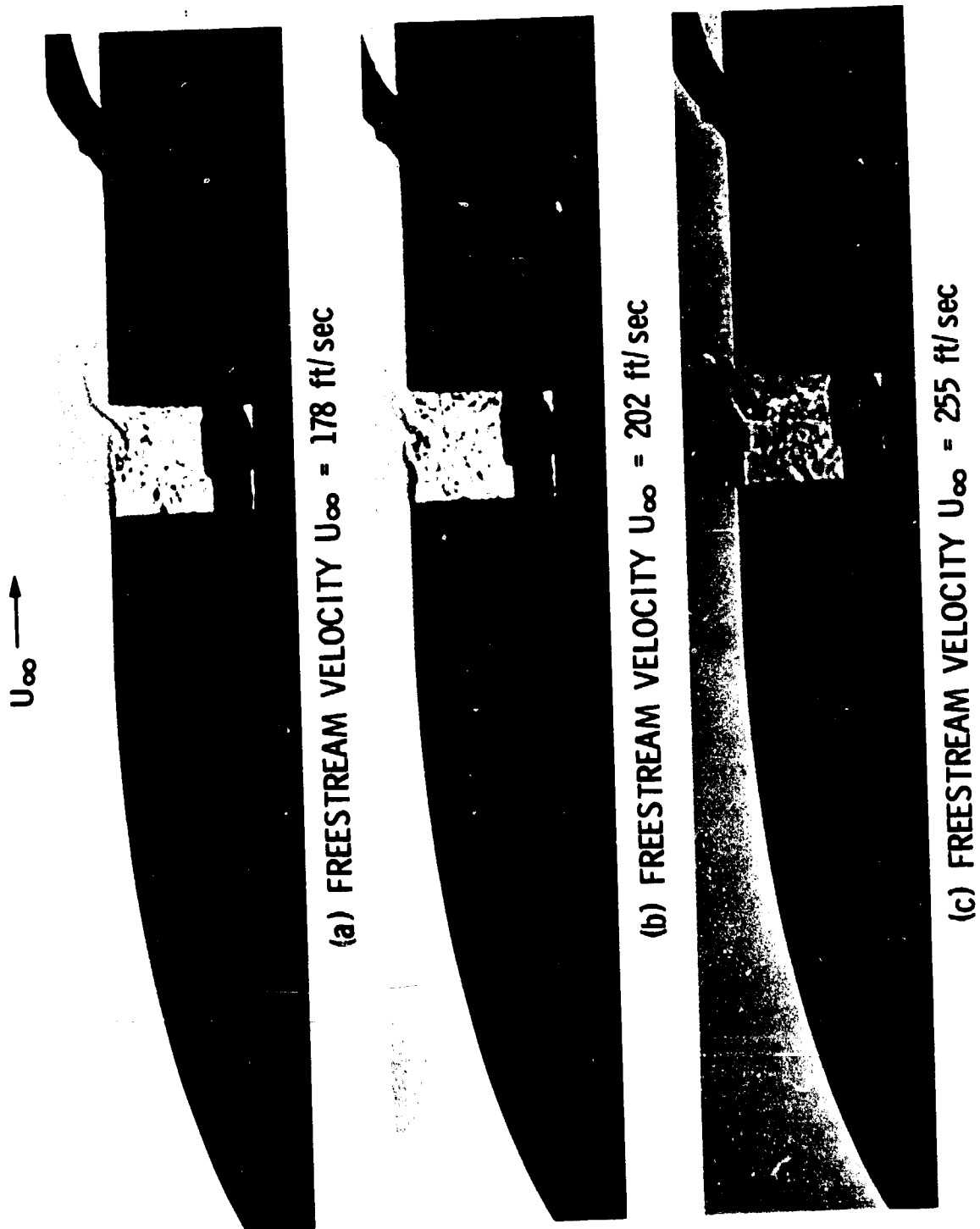FIGURE 12.   FLOW VISUALIZATION WITH LAMINAR BOUNDARY LAYER SEPARATION AT UPSTREAM CAVITY CORNER

$U_\infty \longrightarrow$

(a) FREESTREAM VELOCITY U_∞ = 178 ft/sec

(b) FREESTREAM VELOCITY U_∞ = 202 ft/sec

(c) FREESTREAM VELOCITY U_∞ = 255 ft/sec

FIGURE 13.   FLOW VISUALIZATION WITH TURBULENT BOUNDARY LAYER SEPARATION AT UPSTREAM CAVITY
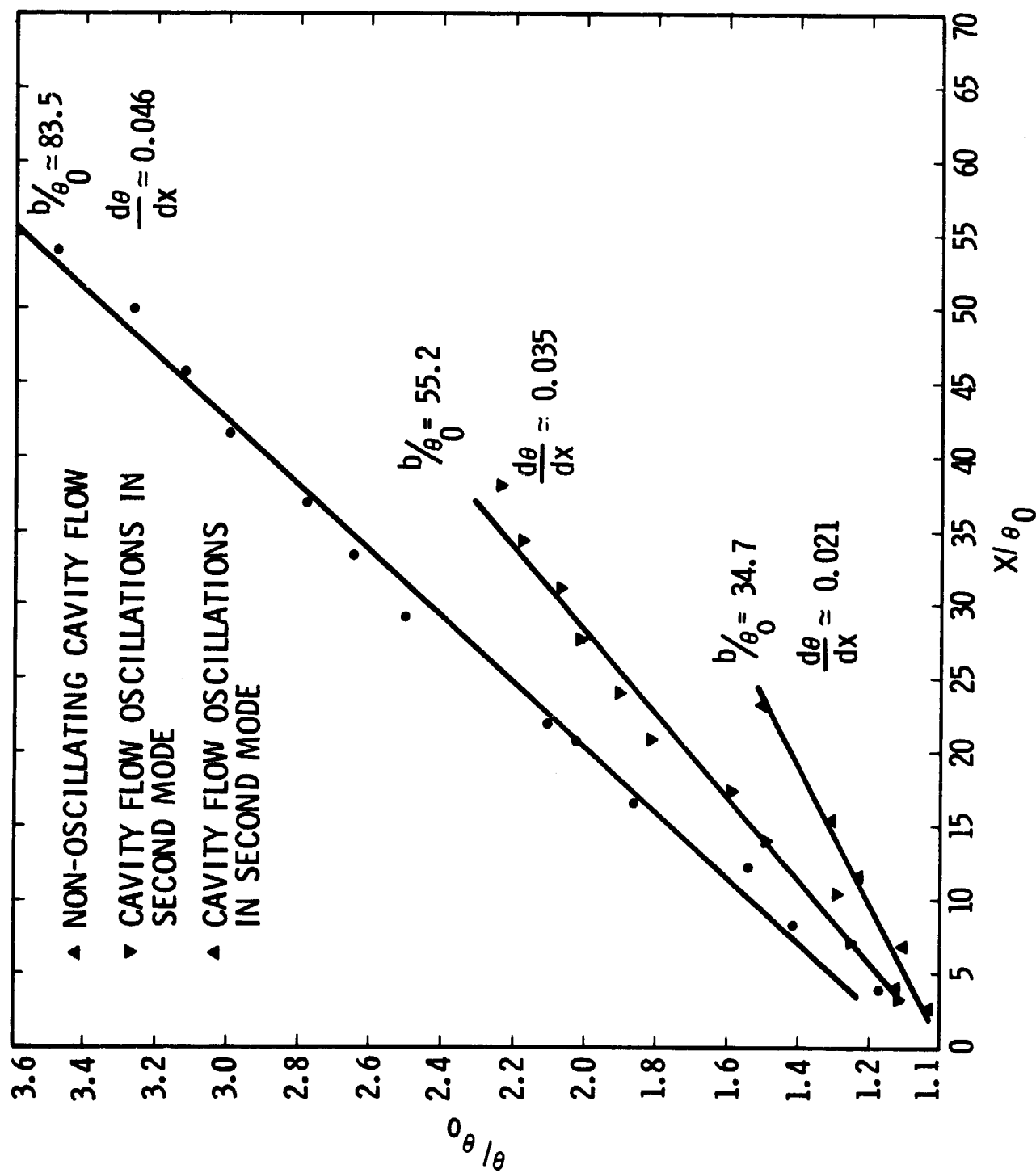
FIGURE 14. EFFECT OF CAVITY WIDTH ON SHEAR LAYER GROWTH AT $Re_{\theta_0} = 1.60 \times 10^3$ AND $d/\theta_0 = 37.5$
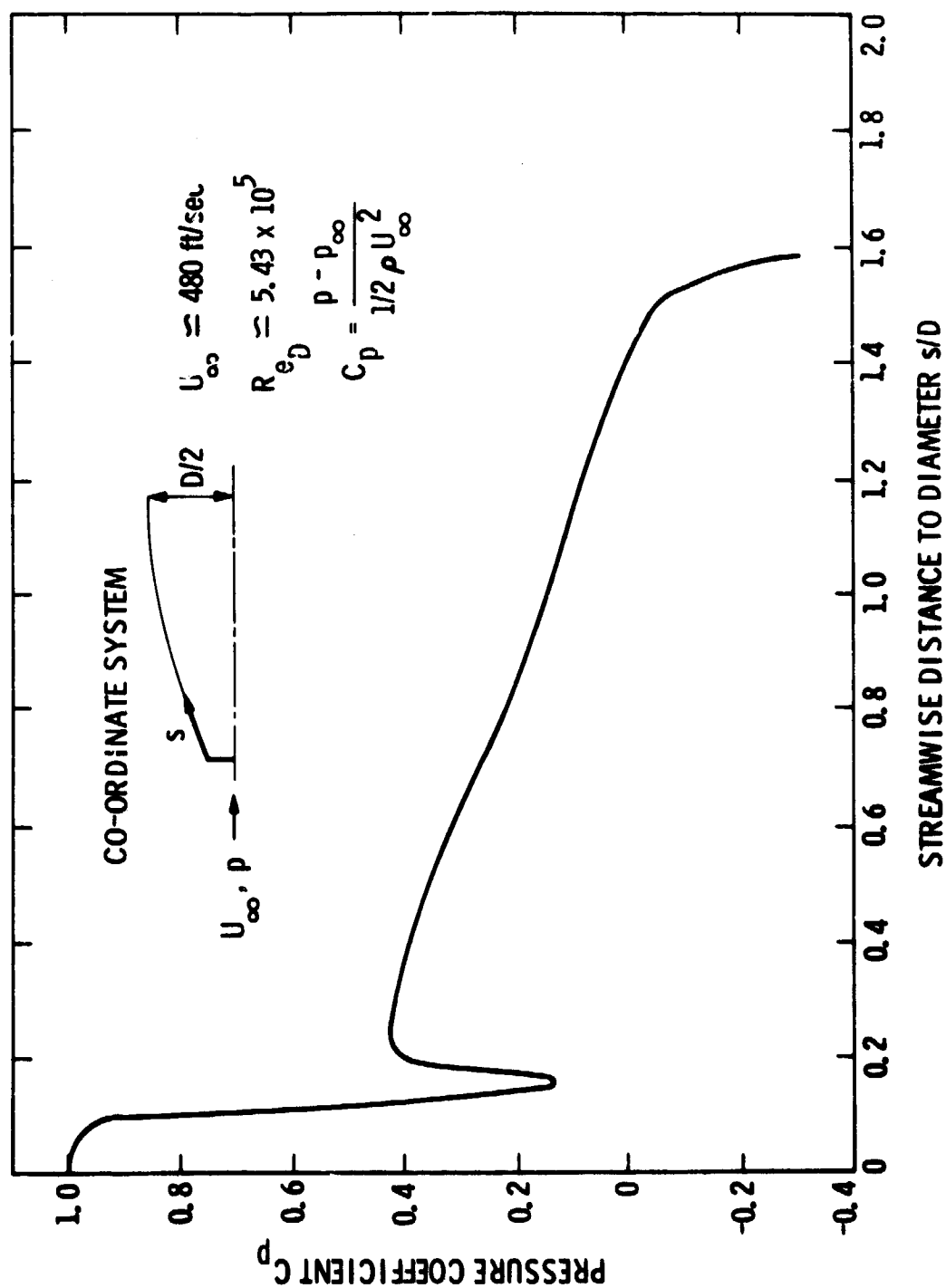
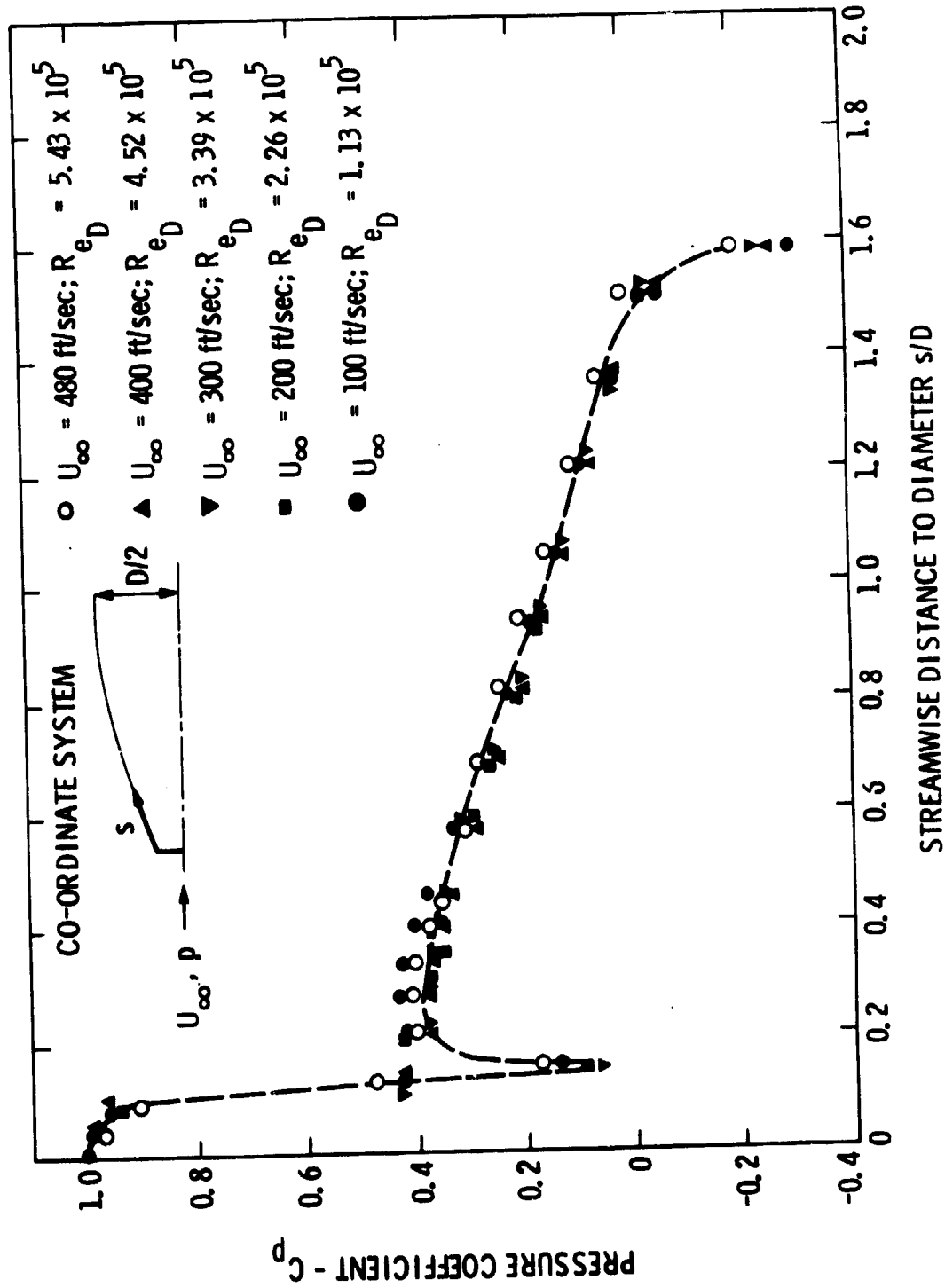FIGURE 15. PRESSURE DISTRIBUTION ON FUSE NOSE CONTOUR

FIGURE 16.   PRESSURE DISTRIBUTION ON FUSE NOSE CONTOUR AT VARIOUS REYNOLDS NUMBERS